PROD. TYPE: COM
PP: 1-20 (col.fig.: nil)
CBM621 DTD VER: 5.0.1
ED: Pradeep
PAGN: Suresh – SCAN: Roopa
ARTICLE IN PRESS

ELSEVIER

Computers in Biology and Medicine ▮▮▮ (▮▮▮) ▮▮▮–▮▮▮

Computers in Biology and Medicine

www.intl.elsevierhealth.com/journals/cobm

An intelligent system for automatic detection of gastrointestinal adenomas in video endoscopy

Dimitris K. Iakovidis[a,*], Dimitris E. Maroulis[a], Stavros A. Karkanis[b]

[a] *Department of Informatics and Telecommunications, University of Athens, Panepistimiopolis, Illisia, 15784 Athens, Greece*
[b] *Department of Informatics and Computer Technology, Technological Educational Institute of Lamia, 3rd km Old National Road, 35100 Lamia, Greece*

Abstract

Today 95% of all gastrointestinal carcinomas are believed to arise from adenomas. The early detection of adenomas could prevent their evolution to cancer. A novel system for the support of the detection of adenomas in gastrointestinal video endoscopy is presented. Unlike other systems, it accepts standard low-resolution video input thus requiring less computational resources and facilitating both portability and the potential to be used in telemedicine applications. It combines intelligent processing techniques of SVMs and color–texture analysis methodologies into a sound pattern recognition framework. Concerning the system's accuracy this was measured using ROC analysis and found to exceed 94%.

Keywords: Biomedical system; Video endoscopy; Color–texture features; Support vector machines; Gastrointestinal lesions; Adenomas

1. Introduction

Gastrointestinal neoplasms include polyps arising from the epithelial cells of the gastric and the colonic mucosa. These polyps are mainly classified into two types: adenomatous and hyperplastic polyps. Polyps of the first type, also referred to as adenomas, are usually cancer precursor lesions, whereas polyps of the second type are not considered to be premalignant. Definitive distinction between the two types requires polyp biopsy and histological examination of the tissue specimens. Although there are modern

* Corresponding author. Tel.: +30 210 7275317; fax: +30 210 7275333.
E-mail address: rtsimage@di.uoa.gr (D.K. Iakovidis).

0010-4825/$ - see front matter © 2005 Elsevier Ltd. All rights reserved.
doi:10.1016/j.compbiomed.2005.09.008

non-invasive procedures to detect polyps, such as virtual endoscopy, standard video endoscopy remains the most efficient minimally invasive procedure to detect even small-size polyps that allows biopsy and in many cases polyp resection. Today, the international consensus for the treatment of polyposis dictates removal of all polyps, regardless of the location, the size or other characteristics, in order to prevent a possible development of cancer [1–3].

During an endoscopic examination it is possible for some polyps to go undetected and evolve into malignant tumors in the following years. A reliable system that would be capable of supporting the detection of adenomas could increase the endoscopist's ability to accurately locate early stage adenomas, and could contribute to the reduction of the duration of the endoscopic procedure, which is in most cases uncomfortable for the patients. Such a system would minimize the expert's subjectivity introduced in the evaluation of the clinical characteristics of the examined tissue. Moreover, a consequent cost reduction of the operation would also be feasible, as more patients could be examined faster even by less experienced personnel.

A variety of methods have been proposed in the literature for computer-aided evaluation of gastrointestinal endoscopic images or video. First attempts include the application of edge detection methods for the detection of gastric ulcers [4], region-growing methods for the extraction of large intestinal lumen contours [5] and for the detection of abnormalities in the lower gastrointestinal tract [6].

By the end of the nineties, texture analysis methods combined with intelligent pattern classification techniques began to arise for the detection of lesions in endoscopic images. These methods were motivated by the fact that the textural characteristics of the tumorous lesions can be used for diagnosis not only microscopically [7] but also macroscopically [8]. Neural network-based grey-level texture analysis approaches of endoscopic images include the usage of texture spectrum [9], co-occurrence matrix [10,11], local binary patterns (LBP) [12] and wavelet- domain co-occurrence matrix features [13]. The latter approach has been applied for tumor detection in colonoscopic video-frame sequences in [14] and it was integrated in a versatile and standalone software system for the detection of colorectal lesions in endoscopic video-frames named CoLD [15].

Although texture has proved to be important for the characterization of colorectal lesions, it has been shown that color can be used as an additional clue for the detection of lesions in endoscopic images. Tjoa and Krishnan [16] combined texture spectrum and color histogram features for the analysis of colon status. Karkanis et al. [17] extended the concept of wavelet-domain co-occurrence matrix features for color images and proposed the color wavelet covariance (CWC) features for computer-aided detection of adenomatous polyps of the colon in high-resolution endoscopic video-frames. The experimental results showed that these features lead to higher detection sensitivity than the original grey-level features and other color–texture descriptors [18]. In a later work, Zheng et al. [19] proposed a clinical decision support system based on a Bayesian fusion scheme that combines color, texture and lumen contour information for the detection of lumps and bleeding lesions in colonoscopic images. The fusion approach led to a marginal improvement of the system's sensitivity and specificity for lump detection as compared with the performance achieved only by extracting grey-level LBP histograms.

In this paper we present a novel intelligent system for automatic detection of colonic and gastric adenomas in endoscopic videos. It utilizes color–texture image features and incorporates non-linear support vector machines (SVMs) to achieve improved detection accuracy compared to the linear classification scheme utilized in [17]. Moreover, we focus on the selection of a feature extraction method appropriate for the analysis of low rather than high-resolution video-frames. The advantages emanating from the adoption of such a method include processing time reduction, applicability in telemedicine and less

demanding hardware requirements. The assessment of the system's performance is realized by means of receiver operating characteristics (ROC), which provide more reliable estimates of accuracy compared to other measures, not deriving from ROC [20], which have been adopted in the previously cited works.

The rest of this paper consists of four sections. Section 2 describes the architecture of the proposed system. The methods investigated for the implementation of each module of the system are described in Section 3. In Section 4, we present the experimental results from the application of the proposed system for the detection of colonic and gastric adenomas, in colonoscopic and gastroscopic videos, respectively. Finally, the conclusions as well as future perspectives of this study are summarized in Section 5.

2. System architecture

The design of the proposed system takes into account the practical needs of both traditional and contemporary endoscopists and allows standard low-resolution video input. The endoscopic examinations or at least the most informative video segments are usually recorded by the endoscopists on standard VHS videotapes, for further, more thorough clinical evaluation. Scarcely do contemporary endoscopists utilize modern digital equipment, which allows direct recording of the endoscopic examination on digital media in standard video file formats (Fig. 1).

The proposed system is implemented in Microsoft Visual $C++$ and it can be installed in most conventional personal computers (PCs) equipped with Microsoft Windows operating system. It accepts video files of the standard AVI format as input, and it outputs characterized video files with markers framing all possible adenomas in the video-frame sequence. It consists of four modules, namely a pre-processing, a feature extraction, a classification and a post-processing module (Fig. 1). In the sequel, the operation of these modules is outlined, and the methods employed in each module are further described in Section 3.

2.1. Pre-processing module

The pre-processing module handles the extraction of video-frames with a user-defined frame rate and size corresponding to a region of interest (ROI) within the original video-frames. This aims to exclusion of irrelevant textual information, such as patient's name, date of birth, date and time of the examination, printed on a constant dark background (Fig. 2). Another task of the pre-processing module is to apply color transformations on the extracted video-frames. The RGB color information they contain can be then transformed to other color models that could enhance the detection of adenomas.

2.2. Feature extraction module

The feature extraction module is assigned to the estimation of color–texture measures from the pre-processed video-frames. More specifically, each frame is raster scanned with a sliding window of user-defined size and sliding step. For each window a number of features are estimated producing this way a single feature vector, as illustrated in Fig. 3. The number of feature vectors produced for each frame depends on its size, the dimensions and the step of the sliding window.

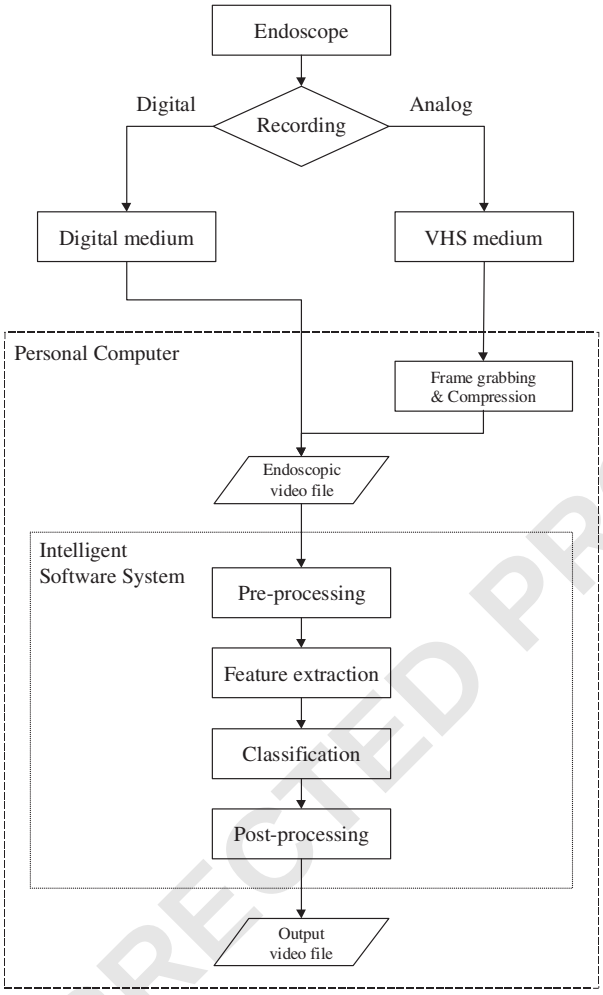

Fig. 1. Block diagram of the proposed system.

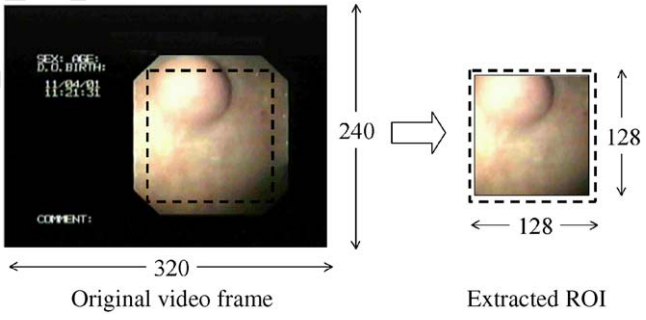

Fig. 2. ROI extraction during pre-processing.

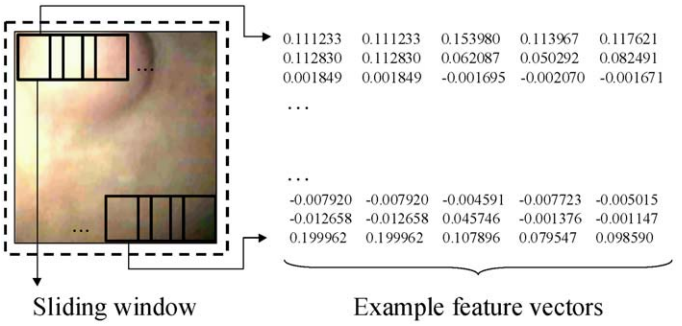

Fig. 3. Feature extraction technique.

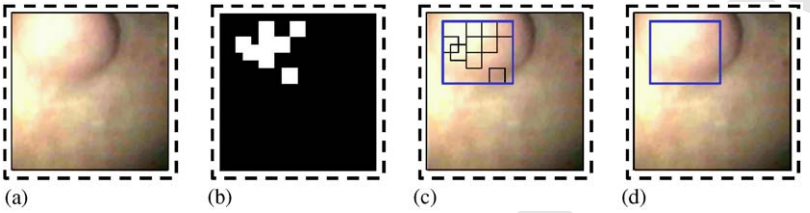

Fig. 4. Post-processing of labeled video-frames: (a) input frame, (b) labeled frame, (c) marker framing the regions labeled as possible adenomas by the classification module, (d) system's output after post-processing.

2.3. Classification module

This module handles the classification of the feature vectors into one of the two classes: adenomas or non-adenomas. The first class usually represents a minority-class of samples, whereas the latter represents a majority-class of samples. In the rest of this document these classes are referred to as normal and abnormal, respectively.

The classification module operates in two modes: the training and the testing modes. The training mode of operation requires that the classification module should be fed with feature vectors from representative video-frames, previously selected and characterized by experts in gastroenterology. During training, the classification module determines its internal parameters based on the available training samples. In the testing mode of operation it utilizes the knowledge gained from the training samples to classify new samples extracted from unknown video-frames. The test samples are forwardly propagated and are consequently labeled as normal or abnormal. For each frame a stream of labels is generated and directed to the post-processing module that follows.

2.4. Post-processing module

The post-processing module utilizes the output of the classification module to produce new video-frames on which the possible adenomas are appropriately marked. The technique applied is illustrated in Fig. 4. The stream of labels inputted to the post-processing module is used for the formation of labeled video-frames. Fig. 4(b) illustrates a labeled frame, on which the white color represents abnormal regions

and the black color represents normal regions. The labeled frame is superimposed with the input frame (Fig. 4a) and a marker is drawn as the outer outline of all the abnormal regions (Fig. 4c, d).

3. Methods

3.1. Color model transformations

Many medical applications utilize color to provide additional information that could enhance the diagnostic accuracy. The most common representation of color in digital imaging is realized by means of the RGB color model. The direct use of the RGB model has proved to be inadequate for the description of clinical and pathological characteristics of tissues for various medical diagnostic tasks, including the detection and diagnosis of early stage lesions in endoscopic images [21,22]. Major drawbacks of the RGB color model include the high correlation among its components and the inconformity with the perceptual mechanisms of the human brain [23].

A variety of color models have been proposed to overcome these drawbacks. These models can be derived from the RGB color model by linear or non-linear transformations implemented in the pre-processing module [17].

3.1.1. Linear transformations

Linear RGB transformations commonly include *XYZ*, *YIQ*, and *K-L* or $I_1I_2I_3$ models [23,24]. Color–texture analysis studies conclude that the use of orthogonal color models improves texture discrimination, with the *YIQ* and *K-L* to be the most prominent models of this type [18]. The *YIQ* model, which is used for NTSC video signal transmission, is nearly orthogonal, whereas *K-L* has been designed to be orthogonal. The *K-L* transform of an image is originally formed by the eigenvector of the image's correlation matrix. Ohta et al. [24] showed that this matrix remains approximately the same for a large set of natural color images and in practice it can be approximated by a linear transformation of the RGB components. The axes of the *K-L* space (I_1, I_2 and I_3) are statistically uncorrelated. I_1 explains the highest proportion of the total variance and represents intensity, whereas I_2 and I_3 correspond to the second and the third highest proportion, respectively, and represent chromatic information.

From a computational point of view the calculation of *K-L* from RGB is far simpler than that of *YIQ*, since it requires simple integer operations [24]. Moreover, it has been experimentally shown that *K-L* leads to a more accurate texture classification than *YIQ*, when used prior to color–texture feature extraction [18], and has been successfully utilized for the detection of adenomas [17].

3.1.2. Non-linear transformations

Two major categories of color models that usually derive from non-linear transformation of the RGB components include the *phenomenal* and the *CIE-uniform* color models [23]. The *phenomenal* color models attempt to classify colors in relation to how they are perceived by the human brain. In general, these color models mainly incorporate hue, saturation and brightness as classifying descriptors, and they are intuitive as regards color manipulation. *CIE-uniform* color models have been proposed to describe color closer to the way it is perceived by humans, in the sense that the Euclidean distances measure the perceived color differences.

The results of previous research on color–texture analysis [18,25] as well as on endoscopic image and video analysis [17] suggest that HSV and CIE-*Lab* color models should be considered in this study, as representative members of the phenomenal and the CIE-uniform color model categories, respectively. HSV consists of hue, saturation and brightness value components, whereas CIE-*Lab* consists of a Lightness component and two chromatic components, a and b.

3.2. Grey-level and color–texture feature extraction

The texture analysis methods have been initially developed for grey-level images mainly because color is not mandatory for the human perception of texture. The effectiveness of the wavelet transform for texture analysis has been pointed out in many studies for texture classification [27,28]. Experiments in color–texture analysis have shown that color information enhances texture classification [29]. Early color–texture analysis approaches mainly involved the extraction of grey-level texture features from each image color channel separately [29]. Recent approaches to color–texture analysis focus on the exploitation of both intra- and inter-channel information [18,30–32].

Motivated by these studies we investigate the performance of three color–texture feature sets, namely the wavelet correlation signatures (WCS), the color wavelet covariance features (CWC) and the opponent color–local binary pattern (OC–LBP) histograms, for the detection of gastrointestinal adenomas in low-resolution endoscopic video. The first two have been applied for the detection of only colonic adenomas in high-resolution video-frames. The last one has been proposed as extension of the LBP for color images [30] and has not been applied for endoscopic image or video analysis in the literature. Moreover, we have considered the extraction of grey-level features such as wavelet energy (WE), LBP and color wavelet energy (CWE) features for comparison purposes.

3.2.1. Wavelet energy features

The discrete wavelet transform (DWT) of a grey-level image is realized by convolution of the image with a low pass filter L and a high pass filter H, the output of which is then sub-sampled dyadically. This procedure produces a low-resolution image $B_0(k)$ and detail images $B_j(k)$, $j = 1, 2, 3$, at scale k, as described by the following equations [33]:

$$\begin{aligned} B_0(k) &= \{L_x * [L_y * B_0(k-1)]_{\downarrow 2x}\}_{\downarrow 2y}, \\ B_1(k) &= \{H_x * [L_y * B_0(k-1)]_{\downarrow 2x}\}_{\downarrow 2y}, \\ B_2(k) &= \{H_x * [H_y * B_0(k-1)]_{\downarrow 2x}\}_{\downarrow 2y}, \\ B_3(k) &= \{L_x * [H_y * B_0(k-1)]_{\downarrow 2x}\}_{\downarrow 2y}, \end{aligned} \tag{1}$$

where $\downarrow 2$ denotes the sub-sampling procedure, x and y denote the row-wise and columnwise operations involved, respectively, and the asterisk (*) is the convolution operator. The repetition of this filtering procedure for $k = 1, 2, \ldots, K$ results in a multiscale representation of the image. The resulting images $B_j(k)$ comprise wavelet coefficients $b^{j,k}$ that encode the content of the input image in variable width spatial frequency bands. By omitting sub-sampling in Eqs. (1), a variation of DWT, the discrete wavelet frame transform (DWFT), is produced [26]. DWFT is a redundant representation that leads to a texture description tolerant to translation [27,28]. The wavelet energy features are estimated by summing the

squares of all $b^{j,k}$ coefficients of the detail images $B_j(k)$, $j = 1, 2, 3$:

$$E^{B_j(k)} = \sum_i b^{j,k}(i)^2. \tag{2}$$

The low-resolution images of the DWFT are not taken into account for the computation of the energies as it has been shown that the detail images at any decomposition level perform better for the characterization of textures than the low-resolution images [34]. A straightforward approach to extract DWFT energy features from color images is to apply DWFT to each color channel C_i and then use Eq. (2) to extract CWE features $E_{C_i}^{B_j(k)}$, $i = 1, 2, 3$, from each color channel C_i of the image separately.

In this study, the DWFT was implemented by using biorthogonal spline filters as they have proved to be more suitable for texture characterization [35].

3.2.2. Wavelet correlation signatures

The WCS have been proposed by Van de Wouwer et al. [18] as extensions of the DWFT energy features that take into account the correlation of the wavelet coefficients between the image color channels. They are derived by the following equation:

$$WC_{C_l,C_m}^{B_j(k)} = \begin{cases} E_{C_l}^{B_j(k)}, & l = m, \\ \dfrac{\sum_i b_{C_l}^{j,k}(i) b_{C_m}^{j,k}(i)}{E_{C_l}^{B_j(k)} \cdot E_{C_m}^{B_j(k)}}, & l \neq m, \end{cases} \tag{3}$$

where $b_{C_l}^{j,k}$ and $b_{C_m}^{j,k}$ are the coefficients of the detail images $B_j(k)$, $j = 1, 2, 3$, $k = 1, 2, \ldots, K$, of the color channels C_l and C_m, $l = 1, 2, 3$, $m = 1, 2, 3$, respectively.

3.2.3. Color wavelet covariance features

The CWC features are covariance estimates of the second-order statistical information inherent in the DWFT of the color channels of an image [17,31,32]. The image color channels are transformed to the wavelet domain by the DWFT. The second-order statistical information of the wavelet coefficients is captured by means of co-occurrence matrices [36]. Co-occurrence matrices encode the grey-level spatial dependence based on the estimation of the second-order joint conditional probability density function $f(i, j, d, a)$, which is computed by counting all pairs of pixels at distance d having grey-levels i and j at a given direction a. The angular displacement of $d = 1$ corresponds to four discrete directions at 0°, 45°, 90° and 135°.

Let $M_{C_i}^{B_j(k)}(a)$ be a co-occurrence matrix estimated over a detail image $B_j(k)$, j=1, 2, 3, k=1, 2, …, K, of the color channel C_i, $i = 1, 2, 3$, for a direction a. Four representative statistical features are estimated over each detail image $B_j(k)$, $j = 1, 2, 3$, $k = 1, 2, \ldots, K$, namely the angular second moment (f_1), the correlation (f_2), the inverse difference moment (f_3) and the entropy (f_4) [36]. The resulting set of features that corresponds to the different color channels C_i is

$$F_{C_i}^{B_j(k)}(a), \quad i = 1, 2, 3, \quad j = 1, 2, 3, \quad k = 1, 2, \ldots, K, \tag{4}$$

where $F \in \{f_1, f_2, f_3, f_4\}$ and $a \in \{0°, 45°, 90°, 135°\}$.

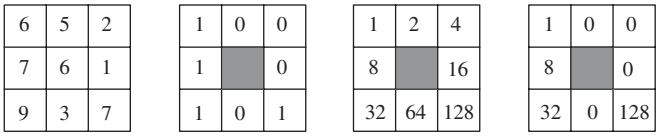

Fig. 5. LBP value estimation: LBP = 1 + 8 + 32 + 128 = 169 [37].

The CWC of a feature F between the detail images $B_j(k)$, $j=1, 2, 3$, $k=1, 2, \ldots, K$, of color channels C_l and C_m, $l = 1, 2, 3$, $m = 1, 2, 3$, is estimated as follows:

$$\mathrm{CWC}_{C_l,C_m}^{B_j(k)} = Cov(F_{C_l}^{B_j(k)}, F_{C_m}^{B_j(k)}), \quad l \leqslant m. \tag{5}$$

3.2.4. Local binary pattern features

The LBP method has been proposed by Ojala et al. [37] as a two-level version of the texture spectrum method [38], which uses three levels (0, 1 and 2) for the representation of local texture patterns. The LBP method utilizes $2^8 = 256$ possible texture units instead of the $3^8 = 6561$ units utilized in the texture spectrum method, leading to a more efficient representation of texture which results in a comparable texture discrimination performance [39]. The local binary pattern of a 3 × 3-pixel neighborhood is estimated as follows:

(i) The original 3 × 3 neighborhood (Fig. 5a) is thresholded to two levels (0 and 1) using the value of the center pixel (Fig. 5b).
(ii) The values of the pixels in the thresholded neighborhood are multiplied by certain weights (Fig. 5c) assigned to the corresponding pixels.
(iii) The values of the eight pixels (Fig. 5d) are summed to obtain a single value for the corresponding pattern.

The LBP feature vectors are formed by histogram bins of the distribution of the LBP values in an image region.

3.2.5. Opponent color—local binary pattern features

The OC–LBP has been proposed by Mäenpää et al. [30] and involves the application of the LBP operator on each color channel separately. In addition, each pair of color channels is used in collecting opponent color patterns so that the center pixel for a neighborhood and the neighborhood itself are taken from different color channels. In total, three intra-channel LBP histograms (one histogram for each color channel C_i, $i=1, 2, 3$) and six inter-channel histograms (for combinations of center-neighborhood pixels: C_1-C_2, C_2-C_3, C_3-C_1, C_2-C_1, C_3-C_2 and C_1-C_3) are extracted and concatenated into a single distribution.

3.3. Classification

A variety of classification algorithms have been proposed in the literature for the realization of intelligent medical applications, including linear discriminant analysis (LDA) [17,40], neural networks [41] and SVMs [45]. The latter are binary classifiers that provide remarkably robust generalization perfor-

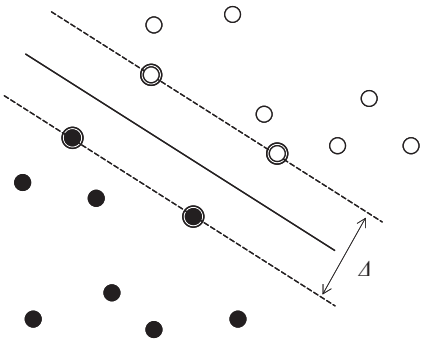

Fig. 6. A linear SVM solution to a linearly separable classification problem.

mance, even with sparse and noisy data. They resist to overfitting the training data and their classification performance is not easily affected by the magnitude of the features-to-samples ratio [42]. Moreover, SVMs are less empirical as regards the determination of their parameters compared to standard neural networks and they have proved to be more accurate than other classifiers in many applications, including the classification of textures [46] and CT colonography patterns [47].

The training of the SVMs involves a quadratic programming optimization procedure which aims at the identification of a subset of vectors from the training set, called *support vectors*. These vectors are utilized for the drawing of a separating hypersurface between two classes. In the case of linearly separable classes, the support vector algorithm searches for the separating hyperplane which leads to the largest possible *margin* Δ between the two classes. A typical example in a two-dimensional feature space is illustrated in Fig. 6. The solid line is the solution hyperplane, the margin Δ is the distance between the two parallel dashed lines, and the outlined black and white samples correspond to the support vectors.

Non-linear classification is based on the idea of injecting the data points into a higher-dimensional Hilbert space via some non-linear mapping Φ, and using the linear support vector algorithm there to separate the training samples. The support vector algorithm in its general form, which includes the non-linear classification of non-linearly separable classes, proceeds as follows [42,43]:

Let I be an input space of vectors x_i, $i = 1, 2, \ldots, N$, distributed to two classes, which are labeled as $y_i \in \{-1, 1\}$. Considering Φ being a non-linear mapping from the input space $I \subseteq \Re^n$ to a Euclidean space E, training the SVM results in a vector $\mathbf{w}$ and a scalar w_0 of a hypersurface defined by the equation

$$\mathbf{w}\Phi(x) + w_0 = 0, \tag{6}$$

so that the margin of separation between the two classes is maximized. It is easy to prove that for the *maximal margin* hypersurface,

$$\mathbf{w} = \sum_{i=1}^{N} \lambda_i y_i \Phi^{\mathrm{T}}(x_i), \tag{7}$$

and w_0 is estimated from the Karush–Kuhn–Tucker *complementarity condition*. The variables λ_i are Lagrange multipliers which are estimated by maximizing the Lagrangian

$$L_D = \sum_{i=1}^{N} \lambda_i - \frac{1}{2} \sum_{i=1}^{N} \sum_{j=1}^{N} \lambda_i \lambda_j y_i y_j K(x_i, x_j), \tag{8}$$

with respect to λ_i. The vectors x_i for which $0 < \lambda_i \leqslant c$ are the *support vectors* and c is a positive cost parameter. As c increases a higher penalty for errors is assigned.

The function $K(x_i, x_j)$ is known as *kernel function* and should satisfy Mercer's condition [43]. It is defined by the following inner product:

$$K(x_i, x_j) = \Phi^{\mathrm{T}}(x_i)\Phi(x_j). \tag{9}$$

Common choices include the linear and the Gaussian radial basis function (RBF) kernel, which are estimated by the following equations, respectively:

$$K(x_i, x_j) = x_i x_j, \tag{10}$$

$$K(x_i, x_j) = \mathrm{e}^{-\|x_i - x_j\|^2/\gamma}, \tag{11}$$

where γ is a strictly positive constant. The Gaussian kernel performs usually better than other non-linear kernels, such as the polynomial, because it usually has a better boundary response as it allows for extrapolation, and most high-dimensional data sets can be approximated by Gaussian- like distributions similar to those used by radial basis function networks [44]. Moreover, it involves only one parameter (γ), and thus facilitates the search for the optimal values of the SVM parameters.

The hypersurface separating the two classes can be finally derived by the following equation:

$$\sum_{\forall i: 1 \leqslant i \leqslant N, 0 < \lambda_i \leqslant c} \lambda_i y_i K(x_i, x) + w_0 = 0. \tag{12}$$

Given a test input vector x, the trained SVM produces an output value s which corresponds to the label of the class it belongs to:

$$s = \mathrm{sign}\left(\sum_{\forall i: 1 \leqslant i \leqslant N, 0 < \lambda_i \leqslant c} \lambda_i y_i K(x_i, x) + w_0 \right), \tag{13}$$

where sign is a function that returns 1 for positive and -1 for non-positive input values.

In the proposed system the SVMs implement the classification module which handles the classification of the feature vectors x_i, extracted from endoscopic video-frames, into normal or abnormal.

4. Results

Extensive experiments were performed towards two directions. The first is the assessment of the accuracy of the proposed system in the detection of gastrointestinal adenomas. The second is the direction of the determination of the most appropriate methods to be employed.

The experiments have been analyzed by applying receiver operating characteristic (ROC) analysis, as it evaluates the classification performance independent of the naturally occurring class distribution or error cost [20,48]. An ROC graph represents on the x-axis the probability that the classification module regards the sample as abnormal when it is actually abnormal, and on the y-axis the probability that the sample is abnormal when it is actually normal. The former is also known as true positive rate (or sensitivity), whereas the latter is also known as false positive rate (or one minus specificity). The ROC curve shows how these two quantities vary together as the decision threshold varies. The area under the ROC curve (AUC) is used as a reliable measure of the classification accuracy [20].

The experiments were performed on a database of 60 colonoscopic and 26 gastroscopic videos from patients examined in the General Hospital of Athens "Laiko", Medical School, University of Athens. All polyps found during the endoscopic examinations went through biopsy and were histologically evaluated. The results of the histological evaluation were used as the gold standard for the evaluation of the proposed system. As the experts suggested, mainly small size adenomas have been considered for the purposes of our study. Such polyps are not easily detectable, they are more common and are more likely to become malignant compared to the hyperplastic polyps [1].

The endoscopic video files were acquired by the endoscopists and saved in AVI format with a resolution of 320 × 240-pixel frame dimensions, 24 bit color depth at a frame rate of 25 fps. The duration of each video was set at 10 s, which results in 250 frames.

For the purposes of our experiments, two training sets were formed from 40% of the frames comprising the available videos. The first set was built from 100 representative video-frames of each colonoscopic video, and the second, from 100 representative video-frames of each gastroscopic video. In total, the corresponding training sets comprised $60 \times 100 = 6000$ colonoscopic and $26 \times 100 = 2600$ gastroscopic video-frames, respectively. These frames were carefully selected by experts in gastroenterology and correspond to adenomas or normal tissue captured from different angles and illumination conditions. A balanced proportion of normal and abnormal samples was extracted from these frames in a way that all abnormal samples were included and an equal number of normal samples was randomly selected. In [48], it has been shown that learning from a balanced class distribution the classifiers generally come up with fewer but more accurate classification rules for the minority class than for the majority class. So, such an approach is expected to enhance the classification of abnormal samples and thus increase the system's sensitivity.

Apart from the training sets, two test sets were formed from the video-frames that were not included in the training sets, i.e. $250 - 100 = 150$ frames (60%) from each video. The first test set comprised $150 \times 60 = 9000$ colonoscopic video-frames, and the second, $150 \times 26 = 3900$ gastroscopic video-frames. Each of these frames was raster scanned by the feature extraction module and all of the occurring samples were used in the corresponding testing phase, regardless of the class they belong to. It should be explicitly stressed that the training and test sets have been chosen so that they do not overlap, and that feature extraction was class-blind, so that the reliability of the presented results is ensured.

The sampling of each frame was performed by the feature extraction module using a sliding window of 32 × 32-pixel dimensions and a sliding step of 16 pixels, resulting in a total of $7 \times 7 = 49$ samples per frame. A 4-level DWFT was considered for the extraction of the WE, CWE and WCS features [18,27], whereas a 1-level DWFT was applied for the extraction of the CWC features [17]. The LBP and OC–LBP histograms were quantized at 64-bins. The dimensions of the feature spaces produced by each feature extraction method are presented in Table 1. These vectors were classified by employing both linear and non-linear Gaussian kernel functions (Eqs. (10)–(11)) in the classification module.

Table 1
Dimensions of the feature spaces tested in the experiments

Feature space	Dimension
WE	13
CWE	39
WCS	72
CWC	72
LBP	64
OC–LBP	576

The results that follow are organized into two parts in accordance with the data sets used in the experiments.

4.1. Detection of colonic adenomas

The application of the proposed system on the colonoscopic data set using different combinations of color models and feature extraction methods produced the average classification results illustrated in Fig. 7. A standard deviation of approximately 0.2% was estimated for the corresponding accuracies.

In the case of linear classification, the use of the *K-L* CWC features results in the highest classification accuracy (93.8%). The accuracy achived with the RGB OC–LBP features is also high, reaching 93.0%. Although the LBP are nine times fewer than the OC–LBP features (Table 1), they lead to 92.0% accuracy. The introduction of non-linearity in the classification module affects positively the performance of all feature sets but to a different extent. Most affected appears to be the accuracy of the wavelet energy features (WE, CWE and WCS). The WE features perform worst in all cases. The accuracy of the 64 LBP features remains close to the performance of the color–texture features, reaching 93.0%. The same accuracy is achieved with only 39 CWE features. The RGB OC–LBP, the *K-L* CWC and the *K-L* WCS features perform best, resulting in 94.5%, 94.4% and 94.2% accuracy, respectively. These percentages could be considered comparable to each other, but the dimensionality of the feature spaces should also be taken into account. Consequently, the OC–LBP features are not preferred, as they are approximately eight times more than the CWC or the WCS features (Table 1).

Expert endoscopists qualitatively evaluated the output videos produced by the proposed system. They validated that the CWC and the WCS feature extraction methods perform equivalently in the *K-L* color space, leading to:

(a) accurate localization of the adenomas within the video-frames,
(b) tight markers surrounding the adenomas.

It is worth noting that the rate of true positive markings counted in the test frames reached 98.8% and the rate of false positive markings reached 1.4%. Four representative output video-frames produced using *K-L* CWC features are illustrated in Fig. 8. These frames were randomly selected from a total of 150 output frames (corresponding to 150 test input frames) of a colonoscopic video. Frames 4, 24, 33 and 96 contain a small tubular adenoma that has been automatically detected and properly marked by the system. Frame 33 does not contain any suspicious lesions, so the system did not produce any markers.

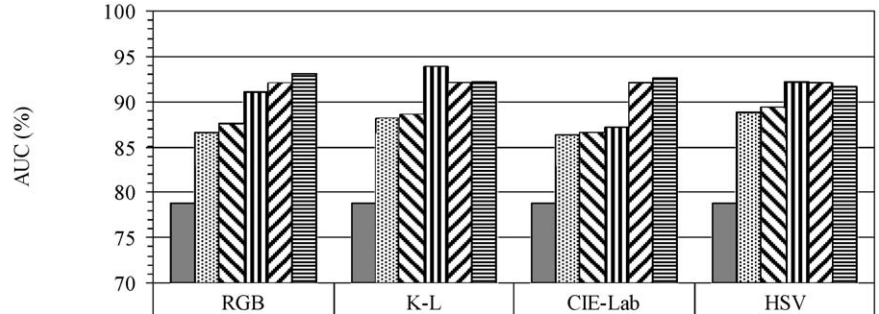

(a)

	RGB	K-L	CIE-Lab	HSV
WE	78.8	78.8	78.8	78.8
CWE	86.5	88.1	86.4	88.8
WCS	87.5	88.6	86.7	89.4
CWC	91.1	93.8	87.2	92.2
LBP	92.0	92.0	92.0	92.0
OC-LBP	93.0	92.1	92.6	91.7

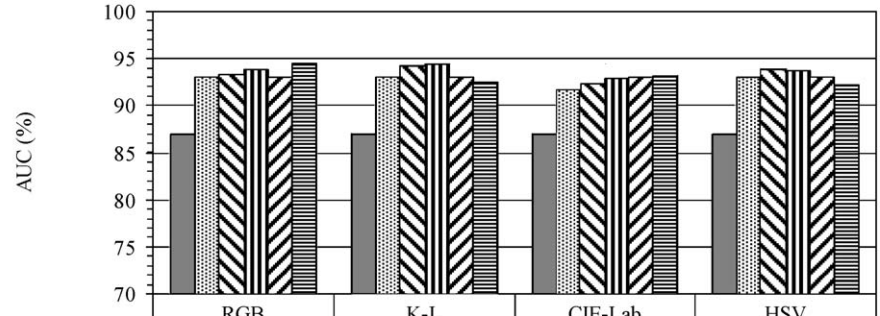

(b)

	RGB	K-L	CIE-Lab	HSV
WE	87.0	87.0	87.0	87.0
CWE	93.0	93.0	91.6	93.0
WCS	93.3	94.2	92.4	93.8
CWC	93.8	94.4	92.8	93.6
LBP	93.0	93.0	93.0	93.0
OC-LBP	94.5	92.5	93.1	92.2

Fig. 7. AUCs obtained for the detection of colonic adenomas using (a) linear and (b) non-linear classification module.

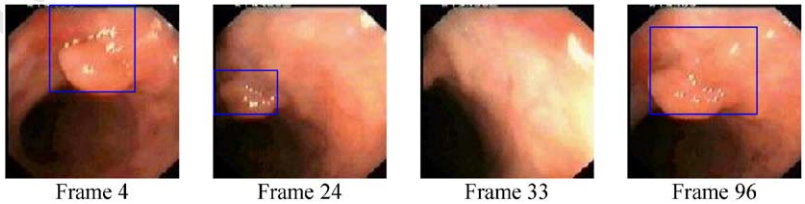

Fig. 8. Output colonoscopic video-frames produced using *K-L* CWC features and non-linear classification.

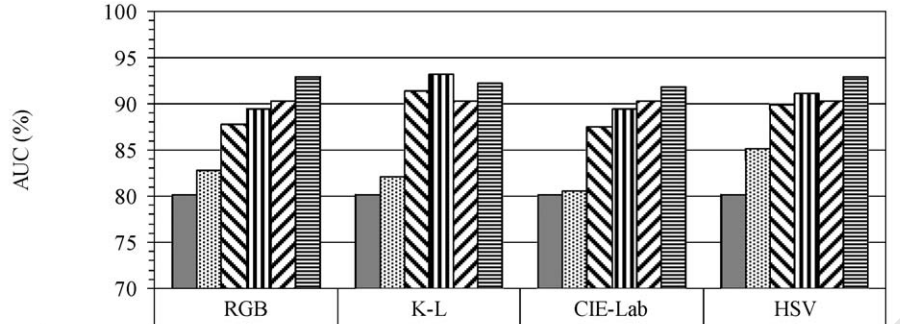

(a)

	RGB	K-L	CIE-Lab	HSV
WE	80.1	80.1	80.1	80.1
CWE	82.7	82.1	80.5	85.2
WCS	87.8	91.4	87.5	89.9
CWC	89.4	93.2	89.4	91.2
LBP	90.2	90.2	90.2	90.2
OC-LBP	92.9	92.2	91.8	92.9

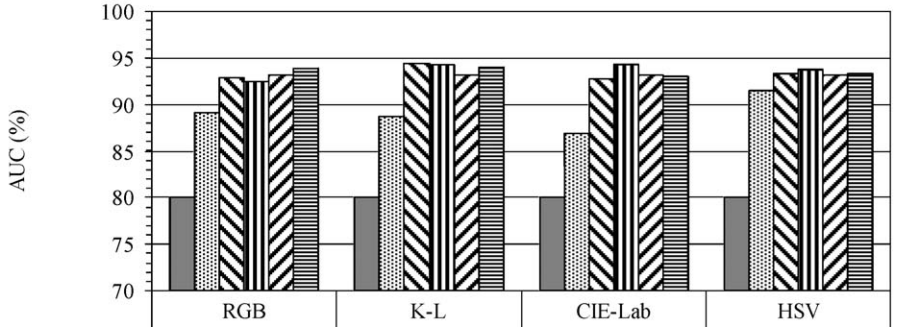

(b)

	RGB	K-L	CIE-Lab	HSV
WE	80.0	80.0	80.0	80.0
CWE	89.1	88.7	86.8	91.5
WCS	92.9	94.4	92.8	93.3
CWC	92.4	94.3	94.2	93.7
LBP	93.2	93.2	93.2	93.2
OC-LBP	93.8	93.9	93.0	93.2

Fig. 9. AUCs obtained for the detection of gastric adenomas using (a) linear and (b) non-linear classification module.

4.2. *Detection of gastric adenomas*

In the second part of the experiments the proposed system was applied for the detection of gastric adenomas, under the previously described framework. The results are illustrated in Fig. 9. A standard deviation of approximately 0.3% was estimated for the corresponding accuracies.

Comparing Fig. 9 with Fig. 7 it can be noticed that the results are almost compatible. The *K-L* CWC features perform best in the case of linear classification leading to 93.2% accuracy. The non-linear

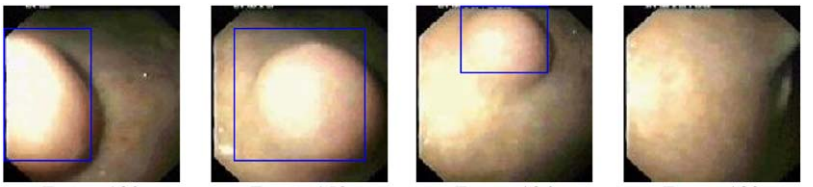

Fig. 10. Output gastroscopic video-frames produced using *K-L* CWC features and non-linear classification.

classification module enhances the classification of the gastroscopic data in most cases and increases the accuracy achieved with the *K-L* CWC and the *K-L* WCS to comparable levels (94.3% vs 94.4%). The WE features do not perform well (80.0%) even with non-linear classification module.

The conclusions of the qualitative evaluation performed by the expert endoscopists on the gastroscopic output videos are in agreement with the conclusions of the respective evaluation performed on the colonoscopic output videos. The rate of true positive markings counted in the test frames reached 97.8% and the rate of false positive markings reached 1.7%. Fig. 10 illustrates a set of representative frames that were randomly selected from a total of 150 output video-frames produced using *K-L* CWC features. A smooth, benign-appearing gastric polyp (close-up view), practically indistinguishable from hyperplastic polyps, was detected in frames 120, 152 and 186. This lesion surprisingly proved to be a tubular adenoma with high-grade dysplasia on biopsy. In frame 189 no lesion appears, so the system did not draw any markers on it.

5. Conclusions

We presented a novel intelligent system capable of supporting the medical decision for detection of adenomas in gastrointestinal video. It aims to the enhancement of the endoscopist's ability to accurately locate early stage adenomas, which may go undetected and evolve into malignant tumors. The system exploits color and textural characteristics of the gastrointestinal epithelium that comprise the clinical findings, which are consequently quantified and used for the development of abstract, mathematically described, decision rules within an SVM classification module.

The results of the extensive experimentation using different color models, feature extraction methods, linear and non-linear classification schemes lead us to the following clear conclusions:

- Textural characteristics of the colonic mucosa can be quantified by measuring texture under the context of image analysis and for the first time color–texture analysis methodologies are successfully applied for automatic detection of gastric adenomas.
- In most of the feature spaces investigated, the use of the non-linear SVM kernel positively affects the discrimination of normal from abnormal samples. Depending on the feature extraction method used, the non-linearity of the kernel function affects classification to a different extent. It could be argued that in the cases of OC–LBP and *K-L* CWC features the classes are almost linearly separable and that the non-linear kernel SVM could be replaced by a simpler linear classifier at the cost of a slight decrease in accuracy. However, this could be reasonable under the framework of a non-medical application. In medical applications, accuracy is crucial as it is associated with diagnosis and it concerns patients' health that can not be jeopardized at the cost of some more computations.

- The optimal configuration of the proposed system includes RGB to *K-L* color transform in the pre-processing module, the CWC or WCS feature extraction module and a non-linear classification module. In this paper the non-linearity in the classification module was introduced with the Gaussian function in the SVM kernel. However, other non-linear kernels, such as the polynomial, could have also worked. The determination or the development of new kernel functions that would optimally solve the gastrointestinal lesion detection problem is a challenging topic for future research.
- The utilization of standard low-resolution input, as it has been considered to meet the practical needs of the endoscopists, provides to the system an advantageous time performance over earlier approaches utilizing frames of higher resolution [17]. The increase in time performance achieved for the lower resolution frames is attributed to the reduction of the computational cost which follows the application of the feature extraction methods on a fewer population of windows per frame and/or the smaller window dimensions used. However, the population of windows per frame and the window size are interdependent system parameters and their choice can affect the detection of the gastrointestinal lesions. Considering the window sampling scheme used in the experiments, a division of the frame dimensions by N will result in an N^2-times reduction of the computational cost. For example, dividing the 1024×1024-pixel frame dimensions [17] by $N = 8$ (Fig. 2), a 64-times reduction of the computational cost is achieved.
- The accuracy of the system exceeds 94% as estimated with ROC analysis in the detection and location of the gastrointestinal adenomas from endoscopic videos.

Future perspectives of this work include further enhancement of the system's accuracy by including other input modalities such as shape information, clinical data, etc. Moreover, the implementation of a software–hardware architecture which will be capable of supporting video endoscopy in real-time seems to be feasible as solutions have been proposed in the literature for the implementation of the feature extraction and the classification modules in hardware [49,50].

6. Summary

Today 95% of all gastrointestinal carcinomas are believed to arise from adenomas. The early detection of adenomas could prevent their evolution to cancer. In this paper we propose a novel intelligent system for automatic detection of gastric and colonic adenomas in endoscopic videos. It utilizes color–texture image features and incorporates non-linear support vector machines (SVMs) to achieve improved detection accuracy compared to the linear classification scheme. The system focuses on the selection of a feature extraction method appropriate for the analysis of low- rather than high-resolution video-frames. The advantages emanating from the adoption of such a method include processing time reduction, applicability in telemedicine and less demanding hardware requirements. The assessment of the system's performance is realized by means of receiver operating characteristics (ROC), which provide more reliable estimates of accuracy compared to other measures. The results of the extensive experimentation on 60 colonoscopic and 26 gastroscopic videos, using different color models, feature extraction methods, linear and non-linear classification schemes, led us to the conclusion that the proposed system can accurately detect, locate and mark the colonic and gastric adenomas within the endoscopic videos provided to its input. Its accuracy exceeds 94% as estimated with ROC analysis.

Acknowledgements

This research was funded by the Operational Program for Education and Vocational Training (EPEAEK II) under the framework of the project "Pythagoras—Support of University Research Groups" co-funded 75% by the European Social Fund and 25% by national funds. We would like to acknowledge Prof. M. Tzivras M.D., Section of Gastroenterology, General Hospital of Athens "Laiko", Medical School, University of Athens and his research group for the provision of the endoscopic videos used in our study and their contribution to the evaluation of the results.

References

[1] S.H. Itzkowitz, Y.S. Kim, Sleisinger & Fordtran's Gastrointestinal and Liver Disease, sixth ed., vol. 2, WB Saunders Company, Philadelphia, 1998.

[2] C.D. Johnson, A.H. Dachman, CT colonography: the next colon screening examination, Radiology 216 (2000) 331–341.

[3] D. Rex, R. Weddle, D. Pound, K. O'Connor, R. Hawes, R. Dittus, J. Lappas, L. Lumeng, Flexible sigmoidoscopy plus air contrast barium enema versus colonoscopy for suspected lower gastrointestinal bleeding, Gastroenterology 98 (1990) 855–861.

[4] H. Kodama, F. Yano, S.P. Ninomija, Y. Sakai, S. Ninomija, A digital imaging processing method for gastric endoscope picture, in: Proceedings of the 21st Annual Hawaian International Conference on System Sciences, vol. 4, 1988, pp. 277–282.

[5] S.M. Krishnan, C.S. Tan, K.L. Chan, Closed-boundary extraction of large intestinal lumen, in: Proceedings of the 16th Annual International Conference of the IEEE Engineering in Medicine and Biology Society, vol. 1, 1994, pp. 610–611.

[6] S.M. Krishnan, X. Yang, K.L. Chan, S. Kumar, P.M.Y. Goh, Intestinal abnormality detection from endoscopic images, in: Proceedings of the International Conference of the IEEE on Engineering in Medicine and Biology Society, vol. 2, 1998, pp. 895–898.

[7] A.N. Esgiar, R.N.G. Naguib, B.S. Sharif, M.K. Bennett, A. Murray, Microscopic image analysis for quantitative measurement and feature identification of normal and cancerous colonic mucosa, IEEE Trans. Inform. Technol. Biomed. 2 (1998) 197–203.

[8] S. Kudo, S. Tamura, T. Nakajima, H. Yamano, H. Kusaka, H. Watanabe, Diagnosis of colorectal tumorous lesions by magnifying endoscopy, Gastrointest. Endos. 44 (1996) 8–14.

[9] S. Karkanis, K. Galousi, D. Maroulis, Classification of endoscopic images based on texture spectrum, in: Proceedings of the Workshop on Machine Learning in Medical Applications, Advance Course in Artificial Intelligence, 1999, pp. 63–69.

[10] S. Karkanis, G.D. Magoulas, M. Grigoriadou, M. Schurr, Detecting abnormalities in colonoscopic images by textural description and neural networks, in: Proceedings of the Workshop on Machine Learning in Medical Applications, Advance Course in Artificial Intelligence, Chania, Greece, 1999, pp. 59–62.

[11] G.D. Magoulas, V.P. Plagianakos, M.N. Vrahatis, Neural network-based colonoscopic diagnosis using on-line learning and differential evolution, Appl. Soft Comput. 4 (2004) 369–379.

[12] P. Wang, S.M. Krishnan, C. Kugean, M.P. Tjoa, Classification of endoscopic images based on texture and neural network, in: Proceedings of the 23rd IEEE Engineering in Medicine and Biology, vol. 4, 2001, pp. 3691–3695.

[13] S.A. Karkanis, G.D. Magoulas, D.K. Iakovidis, D.A. Karras, D.E. Maroulis, Evaluation of textural feature extraction schemes for neural network-based interpretation of regions in medical images, in: Proceedings of the IEEE International Conference on Image Processing, Thessaloniki, Greece, 2001, pp. 281–284.

[14] S.A. Karkanis, D.K. Iakovidis, D.A. Karras, D.E. Maroulis, Detection of lesions in endoscopic video using textural descriptors on wavelet domain supported by artificial neural network architectures, in: Proceedings of the IEEE International Conference on Image Processing, Thessaloniki, Greece, 2001, pp. 833–836.

[15] D.E. Maroulis, D.K. Iakovidis, S.A. Karkanis, D.A. Karras, CoLD: A versatile system for detection of colorectal lesions in endoscopy video-frames, Comput. Methods Programs Biomed. 70 (2003) 151–166.

[16] M.P. Tjoa, S.M. Krishnan, Feature extraction for the analysis of colon status from the endoscopic images, BioMedical Engineering OnLine, 2003, pp. 2–9.

[17] S.A. Karkanis, D.K. Iakovidis, D.E. Maroulis, D.A. Karras, M. Tzivras, Computer aided tumor detection in endoscopic video using color wavelet features, IEEE Trans. Inform. Technol. Biomed. 7 (2003) 141–152.
[18] G. Van de Wouwer, P. Scheunders, S. Livens, D. Van Dyck, Wavelet correlation signatures for color texture characterization, Pattern Recognition 32 (1999) 443–451.
[19] M.M. Zheng, S.M. Krishnan, M.P. Tjoa, A fusion-based clinical decision support for disease diagnosis from endoscopic images, Comput. Biol. Med. 35 (2005) 259–274.
[20] J.A. Swets, R.M. Dawes, J. Monahan, Psychological science can improve diagnostic decisions, Psychol. Sci. Public Interest 1 (2000) 1–26.
[21] Y. Miyake, N. Tsumura, M. Takeya, R. Inagawa, Digital color images in biomedicine, in: H. Tanaka, Y. Miyake, M. Nishibori, D. Mukhopadhyay (Eds.), Japan, 2001.
[22] T. Shiobara, H. Haneishi, Y. Miyake, Improved color reproduction of electronic endoscopes, J. Imaging Sci. Technol. 40 (1996) 494–501.
[23] G. Wyszecki, W.S. Styles, Color Science: Concepts and Methods Quantitative Data and Formulae, Wiley, New York, 1982.
[24] Y. Ohta, T. Kanade, T. Sakai, Color information for region segmentation, in: Proceedings on Computer Graphics and Image Processing, vol. 13, 1980, pp. 222–241.
[25] G. Paschos, Perceptually uniform color spaces for color texture analysis: an empirical evaluation, IEEE Trans. Image Process. 10 (6) (2001) 932–937.
[26] S. Theodoridis, K. Koutroumbas, Pattern Recognition, Academic Press, San Diego, 1999.
[27] M. Unser, Texture classification and segmentation using wavelet frames, IEEE Trans. Image Process. 4 (1995) 1549–1560.
[28] T. Randen, J.H. Husøy, Filtering for texture classification: a comparative study, IEEE Trans. Pattern Anal. Mach. Intell. 21 (1999) 291–310.
[29] A. Drimbarean, P.F. Whelan, Experiments in colour texture analysis, Pattern Recognition Lett. 22 (2001) 1161–1167.
[30] T. Mäenpää, M. Pietikäinen, J. Viertola, Separating color and pattern information for color texture discrimination, Proceedings of the 16th International Conference on Pattern Recognition, Quebec City, Canada, 2002, pp. 668–671.
[31] D.K. Iakovidis, D.E. Maroulis, S.A. Karkanis, I.N. Flaounas, Color texture recognition in video sequences using wavelet covariance features and support vector machines, in: Proceedings of the 29th EUROMICRO Conference, Antalya, Turkey, 2003, pp. 199–204.
[32] D.K. Iakovidis, S.A. Karkanis, D.E. Maroulis, Color wavelet features for texture recognition under varying illumination using support vector machines, in: Proceedings of the IEEE International Conference on Image Processing, Singapore, 2004, pp. 1505–1508.
[33] S.G. Mallat, A theory for multiresolution signal decomposition: the wavelet representation, IEEE Trans. Pattern Anal. Mach. Intell. 11 (1989) 674–693.
[34] W.Y. Ma, B.S. Manjunath, A comparison of wavelet transform features for texture image annotation, Int. Conf. Image Process, 1995, pp. 256–259.
[35] A. Mojscilovic, M.V. Popovic, D.M. Rackov, On the selection of an optimal wavelet basis for texture characterization 9 (2000) 2043–2050.
[36] R.M. Haralick, K. Shanmugam, I. Dinstein, Textural features for image classification, IEEE Trans. Syst. Man Cybern. 3 (1973) 610–621.
[37] T. Ojala, M. Pietikäinen, D. Harwood, A comparative study of texture measures with classification based on feature distributions, Pattern Recognition 29 (1996) 51–99.
[38] D.C. He, L. Wang, Texture unit, texture spectrum, and texture analysis, IEEE Trans. Geosci. Remote Sensing 28 (1990) 509–512.
[39] M. Pietikäinen, T. Ojala, Nonparametric texture analysis with complementary spatial operator, in: M. Pietikäinen (Ed.), Texture Analysis in Machine Vision, Series in Machine Perception and Artificial Intelligence, vol. 40, World Scientific, Singapore, 2000, pp. 3–18.
[40] D. West, V. West, Model selection for a medical diagnostic decision support system: a breast cancer detection case, Artif. Intell. Med. 20 (2000) 183–204.
[41] K. Papik, B. Molnal, R. Schaefer, Z. Dombovari, Z. Tulassay, J. Feher, Application of neural networks in medicine—a review, Diagnostics Med. Technol. 4 (3) (1998) 538–546.
[42] V. Vapnik, Statistical Learning Theory, Wiley, New York, 1998.
[43] C. Burges, A Tutorial on Support Vector Machines for Pattern Recognition, Kluwer Academic Publishers, Boston, 1998.

[44] J. Huang, X. Shao, H. Wechsler, Face pose discrimination using support vector machines (SVM), in: Proceedings of the ICPR International Conference on Pattern Recognition, vol. 1, 1998, pp. 154–156.
[45] I. El-Naqa, Y. Yongyi, M.N. Wernick, N.P. Galatsanos, R.M. Nishikawa, A support vector machine approach for detection of microcalcifications, IEEE Trans. Med. Imaging 21 (12) (2002) 1552–1563.
[46] S. Li, J.T. Kwok, H. Zhu, Y. Wand, Texture classification using the support vector machines, Pattern Recognition 36 (2003) 2883–2893.
[47] S.B. Gokturk, C. Tomasi, B. Acar, C.F. Beaulieu, D.S. Paik, R.B. Jeffrey Jr., J. Yee, S. Napel, A statistical 3-D pattern processing method for computer-aided detection of polyps in CT colonography, IEEE Trans. Med. Imaging 20 (12) (2001) 1251–1260.
[48] G.M. Weiss, F. Provost, The effect of class distribution on classifier learning, Technical Report ML-TR-43, Department of Computer Science, Rudgers University, January 2001.
[49] D. Bariamis, D.K. Iakovidis, D.E. Maroulis, S.K. Karkanis, An FPGA-based Architecture for Real Time Image Feature Extraction, in: Proceedings of the ICPR International Conference on Pattern Recognition, Cambridge, UK, 2004, pp. 801–804.
[50] D. Anguita, A. Boni, S. Ridella, A digital architecture for support vector machines: theory, algorithm, and FPGA implementation, IEEE Trans. Neural Networks 14 (5) (2003) 993–1009.

Dimitris K. Iakovidis received his B.Sc. degree in Physics from the University of Athens, Greece. In April 2001, he received his M.Sc. degree in Cybernetics and in February 2004 his Ph.D. degree in the area of Medical Informatics from the Department of Informatics and Telecommunications, University of Athens, Greece. Currently he is working as a Research Fellow in the same department and he has co-authored more than 30 papers on biomedical applications and image analysis. Also, he is regular reviewer for many international journals. His research interests include biomedical systems, image analysis, pattern recognition and bioinformatics.

Dimitris E. Maroulis received the B.Sc. degree in Physics, the M.Sc. degree in Radioelectricity, the M.Sc. in Electronic Automation and the Ph.D. degree in Informatics, all from the University of Athens, Greece, in 1973, 1977, 1980 and 1990, respectively. In 1979, he was appointed Assistant in the Department of Physics, in 1991 he was elected Lecturer and in 1994 he was elected Assistant Professor, in the Department of Informatics of the same university. He is currently working in the above department in teaching and research activities, including Projects with European Community. His main areas of activity include data acquisition systems, real-time systems, signal processing and biomedical systems.

Stavros A. Karkanis obtained his B.Sc. in Mathematics from the University of Athens, Greece, in April 1986 and his Ph.D. degree in December 1995 from the Department of Informatics and Telecommunications of the same University. For the last 17 years he has been working in the field of image processing, especially in the area of texture recognition from various academic and industry positions. Today he is Associate Professor in the Department of Informatics at the Technological Educational Institute of Lamia. His main interests include texture recognition, wavelet transform for texture, pattern recognition for image processing applications and statistical learning methodologies for classification.